Proceedings of Symposia in Applied Mathematics

Accuracy of stabilized residual distribution for shallow water flows including dry beds

M. Ricchiuto and A. Bollermann

Abstract. We give a further examination of the stabilized Residual Distribution schemes for the solution of the shallow water equations proposed in (Ricchiuto and Bollermann, *J.Comp.Phys.*, available online 25 October 2008). Based on a non-linear variant of a Lax-Friedrichs scheme, the scheme is well-balanced, able to handle dry areas and, for smooth regions of the solution, obtains second order of accuracy. We will analyze the accuracy when dry areas are included in the domain of computation.

1. Introduction

We consider the solution of the two-dimensional shallow water equations, a model for a shallow free surface flow. The only source term we take into account is the elevation of the bottom height, Coriolis and friction forces are neglected. Many problems modeled by the shallow water equations include shorelines, e.g. a transition from flooded to dry areas. This leads to different problems, as the shallow water model loses important mathematical properties. In addition, we face different numerical difficulties when the water height approaches zero.

In [**C**], the authors propose a conservative Residual Distribution scheme which is able to solve the shallow water equations in the described setting. Based on a two-dimensional generalization of the Lax-Friedrichs scheme, the method is extended to a non-linear scheme and provided with a stabilization technique. These measures yield a scheme with second order of accuracy in smooth regions and an essentially non-oscillatory behavior. It is also well-balanced, i.e. steady equilibria between the source term and the flux divergence are exactly reproduced.

Concerning dry bed computations, the reference gives modifications for cells near the front line that allow to simulate the transition between wet and dry areas. These modifications are described to deteriorate the accuracy of the scheme when applied to the whole domain. Although the scheme shows, in general, a very precise representation of the solution for test cases including a wetting/drying front, the overall accuracy is not demonstrated in detail. We want to further investigate this issue in this work, which is organized as follows. In Section 2, we briefly

1991 *Mathematics Subject Classification.* 35L65, 65M12, 76M25, 76B15.

Key words and phrases. Conservative schemes; Residual distribution; Shallow water equations; Unstructured grids.

recall the shallow water equations. This is followed by a description of the residual distribution scheme we use in Section 3, with a somewhat detailed description of the ad-hoc treatment of dry and nearly dry cells in 3.2. We present selected test cases that analyze the effect of these modifications on the accuracy in Section 4 and finally summarize the results in Section 5.

2. The shallow water equations

The shallow water equations in conservation law form read

$$\frac{\partial \mathbf{u}}{\partial t} + \nabla \cdot \boldsymbol{\mathcal{F}}(\mathbf{u}) = \boldsymbol{\mathcal{S}}(\mathbf{u}, \vec{x}) \text{ on } \Omega \times [0, t_f] \subset \mathbb{R}^2 \times \mathbb{R} \tag{2.1}$$

where we have

$$\mathbf{u} = \begin{pmatrix} H \\ Hu \\ Hv \end{pmatrix}, \qquad \boldsymbol{\mathcal{F}} = [\boldsymbol{\mathcal{F}}_1 \, \boldsymbol{\mathcal{F}}_2] = \begin{pmatrix} Hu & Hv \\ Hu^2 + g\frac{H^2}{2} & Huv \\ Huv & Hv^2 + g\frac{H^2}{2} \end{pmatrix}, \tag{2.2}$$

with H the relative water height, $\vec{u} = (u, v)^T$ the vector of velocities and g the gravity constant. The source term is defined as

$$\boldsymbol{\mathcal{S}}(\mathbf{u}, \vec{x}) = -gH \begin{pmatrix} 0 \\ \frac{\partial B(\vec{x})}{\partial x_1} \\ \frac{\partial B(\vec{x})}{\partial x_2} \end{pmatrix}, \tag{2.3}$$

where $B(\vec{x})$ is the bottom elevation. This leads to the *free surface level*, or total water height,

$$H_{tot}(\vec{x}, t) = H(\vec{x}, t) + B(\vec{x}, t).$$

As system (2.1) is hyperbolic, for each direction $\vec{\xi} = (\xi_1, \xi_2)$ the matrix

$$K(\bar{\mathbf{u}}, \vec{\xi}) = \xi_1 K_1(\bar{\mathbf{u}}) + \xi_2 K_2(\bar{\mathbf{u}}) \tag{2.4}$$

has real eigenvalues

$$\lambda_1 = \vec{u} \cdot \vec{\xi} - c, \quad \lambda_2 = \vec{u} \cdot \vec{\xi}, \quad \lambda_3 = \vec{u} \cdot \vec{\xi} + c \tag{2.5}$$

and a full set of linearly independent eigenvectors. Here the K_i denote the flux jacobians

$$K_1 = \frac{\partial \boldsymbol{\mathcal{F}}_1(\bar{\mathbf{u}})}{\partial \mathbf{u}}, \quad K_2 = \frac{\partial \boldsymbol{\mathcal{F}}_2(\bar{\mathbf{u}})}{\partial \mathbf{u}}, \tag{2.6}$$

$c = \sqrt{gH}$ the *speed of sound* and $\bar{\mathbf{u}}$ is some fixed value of $\mathbf{u}$.

3. Residual distribution schemes

To discretize in space, we divide the computational domain Ω in a triangulation $\mathcal{T}_h$ consisting of triangles T with h denoting a reference grid size. The numerical approximation of $\mathbf{u}$ is given by the point values $\mathbf{u}_i = \mathbf{u}(\vec{x}_i)$, where i numbers the nodes of $\mathcal{T}_h$. The linear interpolation between the nodes is referred to as $\mathbf{u}_h$. Similarly, $\boldsymbol{\mathcal{F}}_h$ denotes the approximation to the fluxes. The time will be discretized into time slabs $[t^n, t^{n+1}]$, $n = 0, \ldots, N-1$ with $t^0 = 0$ and $t^N = t_f$ the final time. The time step is given by $\Delta t = t^{n+1} - t^n$.

3.1. A Lax-Friedrichs type scheme. To obtain a numerical solution of (2.1), we use a residual distribution scheme for time-dependent problems. These schemes are based on the *space-time* residual

$$\boldsymbol{\Phi}^T = \int_{t^n}^{t^{n+1}} \int_T \left(\frac{\partial \mathbf{u}_h}{\partial t} + \nabla \cdot \boldsymbol{\mathcal{F}}_h - \boldsymbol{\mathcal{S}}(\vec{x}, \mathbf{u}_h) \right) d\vec{x} dt. \tag{3.1}$$

Assuming linear variation in time of $\mathbf{u}_h$ and $\boldsymbol{\mathcal{F}}_h$, we can write

$$\boldsymbol{\Phi}^T = \frac{|T|}{3} \sum_{j \in T} (\mathbf{u}_j^{n+1} - \mathbf{u}_j^n) + \frac{\Delta t}{2} \left(\boldsymbol{\phi}^T(\mathbf{u}_h^{n+1}) + \boldsymbol{\phi}^T(\mathbf{u}_h^n) \right),$$

where the *local element residual* $\boldsymbol{\phi}^T$ is given by

$$\boldsymbol{\phi}^T(\mathbf{u}_h) = \int_{\partial T} \boldsymbol{\mathcal{F}}(\mathbf{u}_h) \cdot \vec{n} \, dl - \int_T \boldsymbol{\mathcal{S}}(\vec{x}, \mathbf{u}_h) \, dx_1 dx_2. \tag{3.2}$$

Given $\mathbf{u}_h^n$, the solution at the next time step $\mathbf{u}_h^{n+1}$ is defined by the system

$$\sum_{T \in D_i} \boldsymbol{\Phi}_i^T(\mathbf{u}_h) = 0 \quad \forall T \in \mathcal{T}_h \tag{3.3}$$

where the $\boldsymbol{\Phi}_i^T$ form a splitting of $\boldsymbol{\Phi}^T$, i.e.

$$\sum_{j \in T} \boldsymbol{\Phi}_j^T = \boldsymbol{\Phi}^T. \tag{3.4}$$

This implicitly defines matrices $\boldsymbol{\beta}_j$ via

$$\boldsymbol{\Phi}_j^T = \boldsymbol{\beta}_j^T \boldsymbol{\Phi}^T, \quad \sum_{j \in T} \boldsymbol{\beta}_j^T = Id. \tag{3.5}$$

For the definition of the split residuals, we apply a strategy consisting of three steps:

Linear scheme: We define a linear, first order accurate, positive scheme.

Limiting: To achieve higher order of accuracy and keep the positivity, we apply a limiting process to the linear scheme, providing a nonlinear, positive and linearity preserving scheme.

Stabilization: To improve the condition of the problem (3.3) and therewith the quality of the solution in smooth regions, we have to add a stabilization term.

For our numerical examples, we will use the scheme referred to as LLFs in [**C**], which is based on a two-dimensional generalization of the classical Lax-Friedrichs-scheme. We will briefly present the construction of the scheme. For a more detailed derivation and discussion we refer to [**C, B**] and the references therein. We start by defining the local split residuals for the linear scheme

$$\boldsymbol{\phi}_i^{LF} = \frac{1}{3} \boldsymbol{\phi}^T + \frac{1}{3} \alpha \sum_{j \neq i} (\mathbf{u}_i - \mathbf{u}_j), \tag{3.6}$$

where $\alpha \geq \max_{j \in T} \rho(K(\bar{u}, \vec{n}_j))$. $\rho(K)$ the spectral radius of K and $\vec{n}_j$ the inward pointing normal to the edge of node j scaled by the edge length, cf. (2.4). The space-time split residuals used in (3.3) then read

$$\boldsymbol{\Phi}_i^{LF} = \frac{|T|}{3} (\mathbf{u}_i^{n+1} - \mathbf{u}_i^n) + \frac{\Delta t}{2} \left(\boldsymbol{\phi}_i^{LF}(\mathbf{u}_h^{n+1}) + \boldsymbol{\phi}_i^{LF}(\mathbf{u}_h^n) \right). \tag{3.7}$$

The limiting process is now applied to the matrices $\boldsymbol{\beta}_j^{LF}$ implicitly defined via (3.5) and (3.7). The idea is to project the element residual as well as the split residuals to the space given by the eigenvectors of the flux jacobians. We then redistribute the residual according to wether coefficients of the split residuals and the local element residual have the same sign. Formally, we proceed as follows: Let $\mathbf{r}_\sigma$ and $\mathbf{l}_\sigma$ be the right resp. left eigenvectors of $K(\vec{\xi}, \bar{\mathbf{u}}_h)$, cf. (2.4). Here, we choose $\vec{\xi} = (\bar{u}, \bar{v})^T$ for some appropriate average values $\bar{\mathbf{u}}_h$ of $\mathbf{u}_h$. We decompose the residuals as

$$\varphi_\sigma^T = \mathbf{l}_\sigma \boldsymbol{\Phi}^T, \quad \varphi_{\sigma,j}^{LF} = \mathbf{l}_\sigma \boldsymbol{\Phi}_j^{LF} \tag{3.8}$$

and define the distribution coefficients

$$\boldsymbol{\beta}_{\sigma,j}^{LF} := \frac{\varphi_{\sigma,j}^{LF}}{\varphi_\sigma^T}. \tag{3.9}$$

The nonlinear distribution coefficients are then given by

$$\beta_{\sigma,j}^\star = \frac{\max(\beta_{\sigma,j}^{LF}, 0)}{\sum_{i\in T} \max(\beta_{\sigma,i}^{LF}, 0)}. \tag{3.10}$$

We redistribute the decomposed residuals and project them back onto the conservative variables:

$$\varphi_{\sigma,j}^\star = \beta_{\sigma,j}^\star \varphi^T, \quad \boldsymbol{\Phi}_j^\star = \sum_\sigma \varphi_{\sigma,j}^\star \mathbf{r}_j. \tag{3.11}$$

The resulting scheme is positive and linearity preserving. Nevertheless, in practice the scheme shows a poor iterative and grid convergence, with problems occuring in the smooth regions of the solution. This problem was analyzed in [**A**] and the solution proposed there was applied to the scheme at hand in [**C**]. The idea is to add a stabilizing upwind term to the split residuals. The stabilized split residuals take the form

$$\boldsymbol{\Phi}_i^{\star,s} = \boldsymbol{\beta}_i^\star \boldsymbol{\Phi}^T + \epsilon(\mathbf{u}_h) \left(\frac{K_i}{|T|} \tau(\mathcal{T}_h) \boldsymbol{\Phi}^T + \frac{|T|}{36} \sum_{j\in T} D_{ij} (\mathbf{u}_j^{n+1} - u_j^n) \right). \tag{3.12}$$

Here $\epsilon(\mathbf{u}_h)$ is a smoothness sensor to assure that the additional stabilization term is only added in smooth regions of the solution. $\tau(\mathcal{T}_h)$ is a scaling parameter depending on the mesh size and the advection speed. The matrix D takes the form

$$D = \begin{pmatrix} 2 & -1 & -1 \\ -1 & 2 & -1 \\ -1 & -1 & 2 \end{pmatrix}$$

and is introduced by an analogy between residual distribution schemes and Petrov-Galerkin schemes. Details are provided in [**C**].

As a remark, please note that the well-balancing property is based on the exact evaluation of (3.2), such that the flux and the source term cancel each other exactly. The conservation of the scheme is guaranteed by (3.4).

3.2. Modifications for dry bed computations. The treatment of dry boundaries rises a number of new difficulties, demanding changes to the scheme (3.12) at least near the wetting/drying front. More precisely, the following issues have to be addressed:

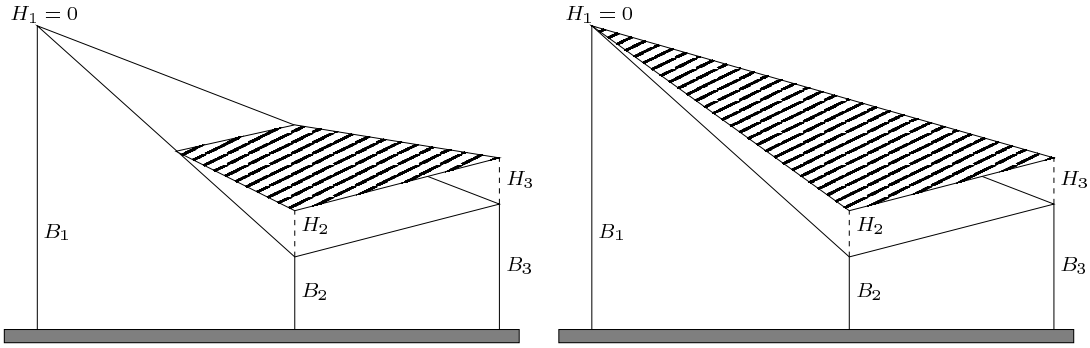

FIGURE 1. Slope in partially dry cell. Left: Physical situation. Right: Numerical interpolation

Positivity: The water height should always be non-negative, i.e. $H_i \geq 0 \quad \forall i$.

Conservation of the lake at rest: Consider the situation in Fig. 1. Due to the linear interpolation of the water height, a non-physical slope of the water height is introduced, leading to spurious velocities at the front between dry and wet nodes.

Undefined velocities: While the conserved quantities H, Hu and Hv are always well defined throughout the computation, the velocities $u = Hu/H$ and $v = Hv/H$ are not necessarily bounded. This can lead to arbitrary velocities near the front.

To ensure the positivity of the water height, we change the limiting process of our scheme. In cells with low water height, we replace φ_σ^T and $\varphi_{\sigma,j}^{LF}$ from (3.8) by

$$\varphi_\sigma^T = \left(\mathbf{\Phi}^T\right)_\sigma \text{ and } \varphi_{\sigma,j}^{LF} = \left(\mathbf{\Phi}_j^{LF}\right)_\sigma . \tag{3.13}$$

In addition, we smoothly switch off the stabilization term from (3.12) via the factor $\epsilon(\mathbf{u}_h)$, which tends to zero for small values of H. In [**C**], it is shown that the resulting scheme keeps the water height positive under a CFL constraint. The authors also give a criterion when one should switch between the two limiters.

For the elimination of spurious velocities due to artificial slopes, we apply an ad-hoc modification to the bottom height. Let $B^{max} := \max_{j \in T} B_j$ be the maximal bottom height in a cell and $H_{tot}^{max} := \max_{j \in T, H_j > 0} H_{tot,j}$. Whenever $B^{max} > H_{tot}^{max}$, for all j with $B_j > H_{tot}^{max}$ we set $B_j = H_{tot}^{max}$, see Fig. 2 for a visualization.

Finally, we cut off velocities if the water height falls below a certain threshold, i.e. we have

$$u = \begin{cases} \frac{Hu}{H} & \text{if } H > C_u \\ 0 & \text{otherwise.} \end{cases} \tag{3.14}$$

We set

$$C_u = \left(\frac{h}{L_{ref}}\right)^2 , \tag{3.15}$$

where $L_{ref} = \max_{i,j \in \mathcal{T}} \|\vec{x}_i - \vec{x}_j\|_\infty$ is the reference size of the computational domain.

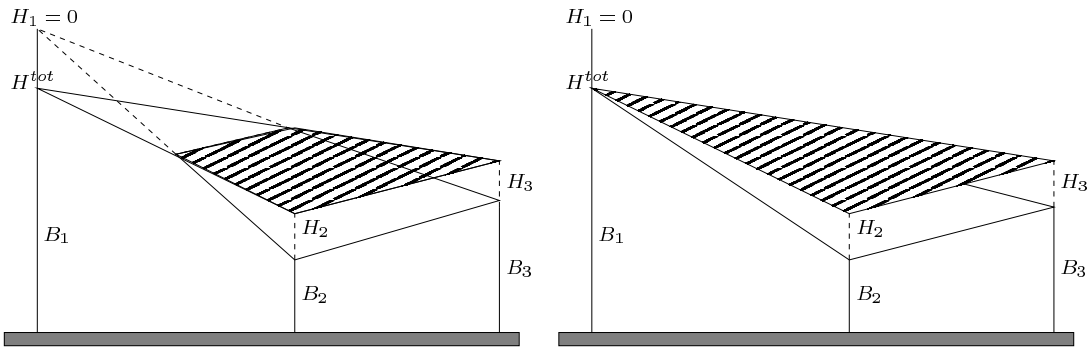

FIGURE 2. Corrected slope in partially dry cell. Left: Real situation with indicated correction. Right: Corrected numerical interpolation

4. Numerical results

The measures proposed in Section 3.2 are necessary to allow computations including dry areas. Nevertheless, the choice of the limiting in characteristic variables has been made for accuracy reasons, and the same is true for the addition of the stabilization term in (3.12), which is dropped near dry zones. We want to investigate how far these modifications in a relatively small part of the computational domain affect the overall solution.

4.1. Accuracy under different limiting strategies. In order to allow a judgement how far the solution is influenced by a partial use of the limiting procedure (3.13), we will present a comparison between the limiting strategies (3.8) and (3.13) applied on the whole computational domain. To suppress any influence created by other modifications, we start by computing a test without the presence of dry areas. The scheme using (3.8) will be referred to as LLFs, like in [**C**], whereas we refer to the SLFs scheme by the one with the simplified limiter (3.13) (no projection).

For the error analysis, we run the the test case of the travelling vortex with both limiters. On a computational domain given by $\Omega = [0,1] \times [0,1]$ we simulate a vortex with center starting at $\vec{x}_C = (0.5, 0.5)$ and moving from left to right with velocity $\vec{u} = (6, 0)$. To the left and right, we apply periodic boundary conditions whereas at the top and bottom the boundary is set to weak far field conditions. The initial solution is given by

$$h_0(r_C) = 10 + \begin{cases} \frac{1}{g}\left(\frac{15}{\omega}\right)^2 (h(\omega r_C) - h(\pi))\big) & \text{if } \omega r_C \leq \pi \\ 0 & \text{otherwise} \end{cases}$$

with

$$h(x) = 2\cos(x) + 2x\sin(x) + \frac{1}{8}\cos(2x) + \frac{x}{4}\sin(2x) + \frac{12}{16}x^2$$

and

$$\vec{u}_0 = \begin{pmatrix} 6 \\ 0 \end{pmatrix} + \begin{cases} 15(1+\cos(\omega r_C))(0.5 - x_2, x_1 - 0.5)^T & \text{if } \omega r_C \leq \pi \\ 0 & \text{otherwise} \end{cases},$$

r_C denoting the distance from $\vec{x}_C$. ω is an angular wave frequency, which we set to $\omega = 4\pi$ and the gravitational constant is chosen as $g = 1$ for this case.

h	$\|H_h - H\|_\infty$	EOC	$\|H_h - H\|_1$	EOC	$\|H_h - H\|_2$	EOC
2.50e-02	1.1686e+00		7.033e-02		1.7448e-01	
1.25e-02	3.5411e-01	1.72	2.1350e-02	1.72	4.9245e-02	1.83
6.25e-03	9.5747e-02	1.89	5.5080e-03	1.95	1.2279e-02	2.01

TABLE 1. Grid convergence for the travelling vortex, LLFs scheme. Error and experimental order of convergence displayed

h	$\|H_h - H\|_\infty$	EOC	$\|H_h - H\|_1$	EOC	$\|H_h - H\|_2$	EOC
2.50e-02	1.8383e+00		9.0911e-02		2.3507e-01	
1.25e-02	6.4433e-01	1.51	3.1523e-02	1.53	7.5674e-02	1.64
6.25e-03	2.6262e-01	1.29	1.0161e-02	1.63	2.4688e-02	1.62

TABLE 2. Grid convergence for the travelling vortex, SLFs scheme. Error and experimental order of convergence displayed

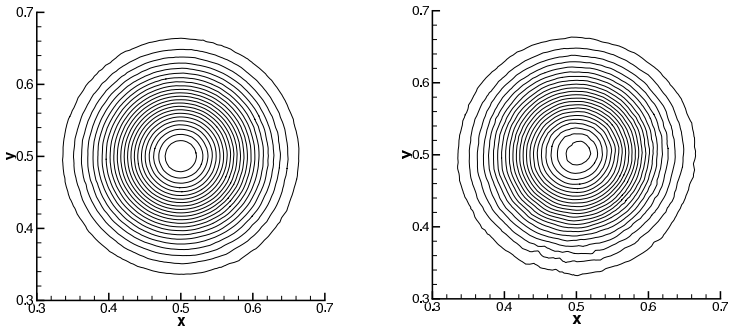

FIGURE 3. Travelling vortex. Contour lines of water height. Left: LLFs scheme. Right: SLFs.

In tables 1 and 2 we present convergence histories for the travelling vortex for both limiting approaches. We can clearly see that the error is always bigger for the SLFs scheme. This alone could be justified by the fact that (3.13) is faster to compute than (3.8), but the real problem is that with this approach we do not reach the expected order of convergence. On the contrary, the scheme obtained using the characteristic projection shows second order of accuracy, whereas the scheme without the projection does not exceed an order of about 1.6. The contour lines in Fig. 3 also show a perturbed solution for SLFs method. It is by far better than the results from the unstabilized scheme presented in [**C**], but clearly inferior to the case with limiting in characteristic variables.

4.2. Grid convergence including dry boundaries. Another point that was left open in [**C**] is an error analysis in presence of dry zones. We recall here a 2D periodic solution of Thacker, namely the curved surface on a parabolic basin.

h	$\|H_h - H\|_\infty$	EOC	$\|H_h - H\|_1$	EOC	$\|H_h - H\|_2$	EOC
6.67e-02	6.4640e-03		4.4344e-03		1.2074e-02	
4.00e-02	3.6123e-03	1.14	1.8420e-03	1.72	5.4764e-03	1.55
2.00e-02	2.2729e-03	0.67	6.0526e-04	1.61	2.2233e-03	1.30
1.50e-03	1.8363e-03	0.74	3.8397e-04	1.58	1.5092e-03	1.34
1.00e-03	1.3447e-03	0.77	1.9916e-04	1.62	8.4688e-04	1.43

TABLE 3. Grid convergence for Thackers curved solution, error and experimental order of convergence displayed. Measured on $\Omega = [-2, 2]^2$, LLFs scheme.

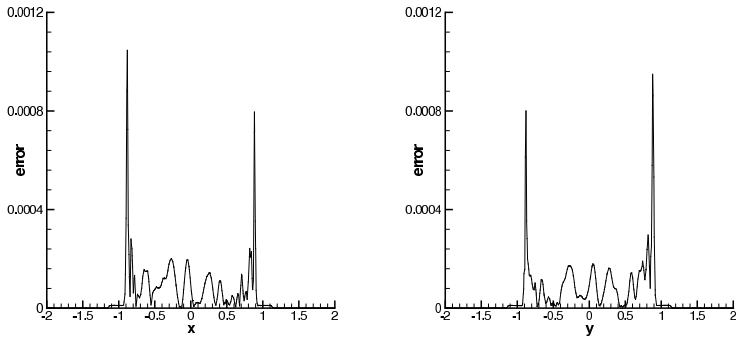

FIGURE 4. $|H_h - H|$ of Thackers curved solution at $t = T$, LLFs scheme. Left: $y = 0$. Right: $x = 0$.

We define the function

$$f(r_c, t) = H_0 \left(-1 + \frac{\sqrt{1 - A^2}}{1 - A\cos(\omega t)} - \frac{r_c^2}{a^2} \left(1 - \frac{1 - A^2}{(1 - A\cos(\omega t))^2} \right) \right),$$

where r_c is a radius, $\omega = \sqrt{8gH_0/a^2}$ the frequency, a a parameter and for a given $r_0 > 0$, A is the shape parameter

$$A = \frac{a^2 - r_0^2}{a^2 + r_0^2}.$$

We then define the bottom height

$$B(\vec{x}) = B(r_c) = -H_0 \left(1 - \frac{r_c^2}{a^2} \right).$$

An analytical solution for the water height is then $H(\vec{x}, t) = \max(f(r_c, t), 0)$. For our computation we set $a = 1$, $r_0 = 0.8$ and $H_0 = 0.1$, such that we get a period $T \approx 2.22$. We compute the solution on the domain $\Omega = [-2, 2]^2$ for different mesh sizes h.

Once again, we computed the case with both limiting approaches until $t = T$, i.e. for one period, and determined the difference between the numerically computed water height H_h and the exact solution H. The error in different norms and the experimental order of convergence is presented in table 3 for the LLFs scheme and in

h	$\|H_h - H\|_\infty$	EOC	$\|H_h - H\|_1$	EOC	$\|H_h - H\|_2$	EOC
6.67e-02	4.9214e-03		3.0119e-03		8.0240e-03	
4.00e-02	3.5363e-03	0.65	1.4930e-03	1.37	4.5919e-03	1.09
2.00e-02	3.5278e-03	0.00	9.1937e-04	0.70	2.9117e-03	0.66
1.50e-02	2.1592e-03	1.70	5.9943e-04	1.48	1.8987e-03	1.48
1.00e-02	1.7278e-03	0.55	3.7553e-04	1.16	1.2523e-03	1.03

TABLE 4. Grid convergence for Thackers curved solution, error and experimental order of convergence displayed. Measured on $\Omega = [-2, 2]^2$, SLFs scheme.

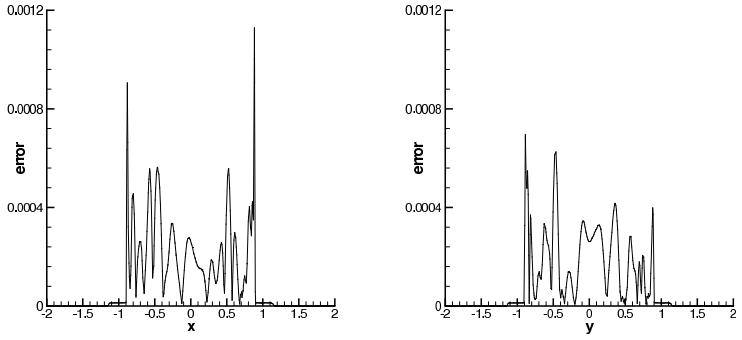

FIGURE 5. $|H_h - H|$ of Thackers curved solution at $t = T$, SLFs scheme. Left: $y = 0$. Right: $x = 0$.

table 4 for the SLFs scheme. In both cases, we see that the order of convergence has dropped compared to the case without dry areas. Nevertheless the grid convergence of the LLFs scheme is much better, especially for the L_1 norm. The SLFs scheme converges very badly. The order of convergence jumps between 0.7 and 1.5, showing no asymptotic behavior.

A possible explanation for the difference in the order of convergence between the L_1 norm on the one hand and the L_{inf} and L_2 norm on the other hand is presented in Fig. 4, where we show $|H_h - H|$ along the lines $x = 0$ and $y = 0$. Next to the wetting/drying front, where the switch between limiting in characteristic and conservative variables takes place, the error is about five times higher than in the central region. The same diagram for the SLFs scheme is shown in Fig. 5. Here the error distribution is much more uniform, though the average error is bigger.

As a final result, we want to check how strong the interior region of the computational domain is influenced by the wetting/drying front. We therefore present the evolution of the error on the circle $\Omega_C = \{\vec{x} : \|\vec{x}\|_2 < 0.75\}$ in table 5. The results for the L_1 norm are quite close to the error on the whole domain Ω, but the L_2 error is now of the same order as the L_1 error. So the overall accuracy is much better than for the SLFs scheme and the error introduced at the boundaries does not affect the interior solution in full strength.

h	$\|H_h - H\|_\infty$	EOC	$\|H_h - H\|_1$	EOC	$\|H_h - H\|_2$	EOC
6.67e-02	3.4289e-03		2.0530e-03		2.4305e-03	
4.00e-02	1.3636e-03	1.81	8.7285e-04	1.67	1.0187e-03	1.70
2.00e-02	5.4830e-04	1.31	2.6821e-04	1.70	3.2462e-04	1.65
1.50e-02	3.8148e-04	1.26	1.6750e-04	1.63	2.0649e-04	1.57
1.00e-02	2.4817e-04	1.06	8.8402e-05	1.58	1.0915e-04	1.58

TABLE 5. Grid convergence for Thackers curved solution, error and experimental order of convergence displayed. Measured on $\Omega_C = \{\vec{x} : \|\vec{x}\|_2 < 0.75\}$, LLFs scheme.

5. Conclusions

We presented the LLFs scheme from [**C**] and its modification for dry beds. In the results section, we gave numerical proof for the necessity to perform the limiting in characteristic variables. We also studied the influence of the dry bed modifications to the overall accuracy. The LLFs scheme showed a nice handling of the wetting/drying front, with mostly localized errors near the front.

References

[A] R. Abgrall, *Essentially non-oscillatory residual distribution schemes for hyperbolic problems*, Journal of Computational Physics **214** (2006), no. 2, 773–808.

[B] Mario Ricchiuto, Remi Abgrall, and Herman Deconinck, *Application of conservative residual distribution schemes to the solution of the shallow water equations on unstructured meshes*, Journal of Computational Physics **222** (2007), 287–331.

[C] Mario Ricchiuto and Andreas Bollermann, *Stabilized residual distribution for shallow water simulations*, Journal of Computational Physics (2008), doi:10.1016/j.jcp.2008.10.020

INRIA BORDEAUX - SUD-OUEST, PROJET SCALAPPLIX, 351 COURS DE LA LIBRATION, 33405 TALENCE CEDEX FRANCE

E-mail address: ricchiuto@inria.fr

IGPM, RWTH AACHEN, TEMPLERGRABEN 55, 52056 AACHEN, GERMANY

E-mail address: bollermann@igpm.rwth-aachen.de